Extremely Narrow Band in Moiré Photonic Time Crystal

Zhaohui Dong,[1] Xianfeng Chen,[1,2] and Luqi Yuan[1,*]

[1]State Key Laboratory of Photonics and Communications, School of Physics and Astronomy, Shanghai Jiao Tong University, Shanghai 200240, China

[2]Collaborative Innovation Center of Light Manipulation and Applications, Shandong Normal University, Jinan 250358, China

(Received 16 December 2024; revised 15 June 2025; accepted 23 June 2025; published 15 July 2025)

The moiré superlattice has attracted growing interest in the electromagnetic and optical communities. Here, we extend this concept to time-varying photonic systems by superposing two binary modulations on the refractive index with different modulation periods, i.e., the moiré photonic time crystal (PTC). Such a moiré PTC leads to extremely narrow bands in momentum space that support temporal localized modes, exhibiting periodically self-reconstructing pulses in the time domain. We investigate the tunability of the band structure of the moiré PTC and the temporal localization behavior, which can be greatly manipulated by varying the temporal modulation parameters. Moreover, we explore the Floquet mode-locking mechanism in the moiré PTC, which points toward potential applications in mode-locked lasers with a tunable time width of the generated pulses. The modulation-induced extremely narrow band also offers intriguing opportunities in exceptional-point-enhanced sensing. Our Letter brings the concept of moiré patterns to the field of PTCs, and unveils new possibilities in wave manipulations with time-varying systems.

DOI: 10.1103/4lqd-z567

The concept of moiré superlattices provides a new degree of freedom in the design of photonic crystals [1–3], which creates intriguing opportunities in wave manipulations such as the localization of light fields [4–9], moiré nanolaser arrays [10–12], tunable optical solitons [13,14], and moiré bound states in the continuum [15,16]. With conventional photonic crystals, distributions of the refractive index of materials are composed spatially in periods. These crystals have a temporal counterpart, i.e., photonic time crystals (PTCs), in which interest has been growing recently [17–19]. PTC systems hold spatial homogeneity while being periodically modulated in the time domain. Unlike a spatial photonic crystal that opens band gaps in the energy axis, the temporal modulation in PTCs causes the interference of time-refracted and time-reflected waves, giving rise to Floquet modes and opening band gaps in the momentum axis [20–24]. In particular, such Floquet modes in the momentum band gaps of PTCs support exponential growing (decaying) features [21–24] due to the time-translation symmetry breaking from temporal modulations, which hence violates energy conservation. Therefore, this naturally piques interest in the study of the temporal analog of the spatial moiré superlattice, i.e., the moiré PTC. For example, the spatial moiré superlattice supports flat bands with zero group velocity and leads to spatial localization modes [25–27]. Correspondingly, it is easy to expect that a moiré PTC shall support extremely narrow bands with a giant group velocity and temporal localized modes according to the space-time duality, which has yet to be fully studied.

In this Letter, we theoretically study a moiré PTC by considering the spatially uniform optical material undergoing the superposition of two binary modulations with different modulation periods. Extremely narrow bands in the momentum axis and the temporal localized modes are explored, where we find that they support periodically self-reconstructing pulses in time. The influence of the modulation parameters on the narrowness of the bands and the temporal width of the localized modes are investigated, which points toward the important development of a Floquet mode-locked lasing mechanism from the physics of moiré PTCs. The modulation-induced extremely narrow band also offers a new way to enhance the sensitivity around exceptional points (EPs).

To construct a moiré PTC, we recall the formation of a spatial one-dimensional (1D) moiré superlattice in Fig. 1(a) by merging two 1D photonic crystals with different spatial periods into a single layer. The moiré PTC is constructed in a similar way by superposing two binary PTCs of different time-varying refractive index patterns, $n_1(t)$ and $n_2(t)$, at modulation periods T_1 and T_2, respectively [see Fig. 1(b)]. Here, a modulation period of $n_1(t)$ [$n_2(t)$] consists of two time segments T_1 (T_2) with time durations τ_a^1 (τ_a^2) and τ_b^1 (τ_b^2) for maximum ($n_{\max}$) and minimum ($n_{\min}$) values of the refractive index, respectively. We set $n_{\min} = 1$ for the simplicity; $n_{\max} = n_{\min} + \Delta n$, where Δn is the modulation strength, and the filling ratio $\tau_a^1/T_1 = \tau_a^2/T_2 = 0.5$. Moreover, we assume modulation periods for the two binary PTCs satisfying $T_1/T_2 = N_1/N_2$, where N_1 and

*Contact author: yuanluqi@sjtu.edu.cn

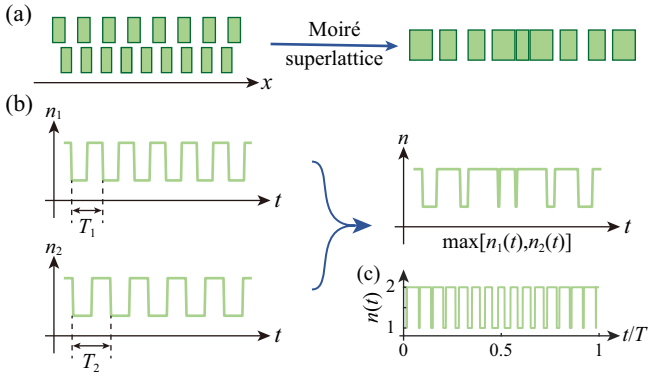

FIG. 1. Schematic illustration of the construction of a moiré superlattice in (a) space domain and (b) time domain. (c) Modulation pattern $n(t)$ for a moiré PTC with $N_1 = 15$, $N_2 = 16$, $n_{\min} = 1$, and $n_{\max} = 2$.

N_2 are coprime numbers. The resulting moiré PTC is then governed by a spatially uniform but time-varying refractive index, $n(t) = \max[n_1(t), n_2(t)]$, with the temporal period $T = N_1 T_2 = N_2 T_1$.

We study the band structure of moiré PTCs [see Supplemental Material (SM) for method [28]]. We take a typical example of the moiré PTC [see Fig. 1(c)] with parameters $N_1 = 15$, $N_2 = 16$, $n_{\min} = 1$, $n_{\max} = 2$ ($\Delta n = 1$), and plot the band structure in Fig. 2(a). One can see the existence of an extremely narrow band (represented by the violet line) in the vicinity of $k_n = 10.8672 k_0$ with a superluminal group velocity, namely, the group velocity is

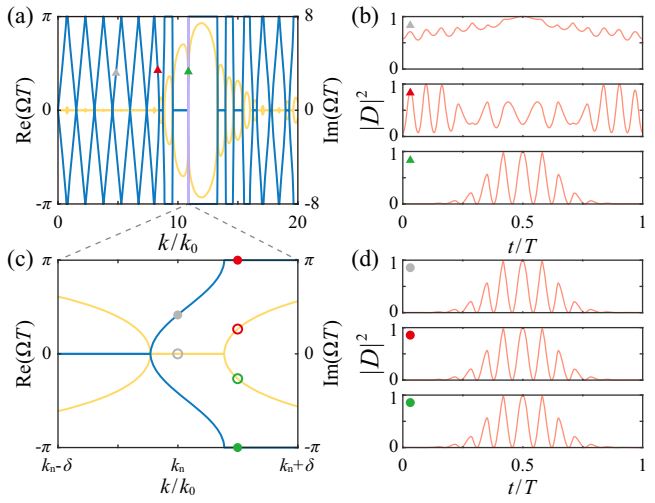

FIG. 2. (a) Band structure of the moiré PTC with $N_1 = 15$, $N_2 = 16$, $n_{\max} = 2$, and $n_{\min} = 1$, where the blue (yellow) lines denote the real (imaginary) part of eigenvalues, i.e., Re(Ω) [Im(Ω)]. (b) Intensity distributions of the electric displacement field $|D|^2$ for the modes denoted in (a). (c) Enlargement of the band structure in (a) in the vicinity of the narrow band, where $\delta = 0.0048 k_0$. (d) Intensity distributions of the electric displacement field $|D|^2$ for the modes denoted in (c), where solid (hollow) circles denote Re(Ω) [Im(Ω)].

faster than the effective speed of light in the moiré PTC. Here, $k_0 \equiv 2\pi/Tc$, with c being the speed of light in vacuum. Such an extremely narrow band originates from the small mismatch between T_1 and T_2. Generally, a single set of modulation $n_1(t)$ produces sidebands from the original bands of the effective static medium, and introduces the coupling between different orders of sidebands, therefore opening momentum band gaps [23,30]. When a second set of modulation $n_2(t)$ is introduced, the small mismatch between T_1 and T_2 induces a severe folding of bands and an extremely small frequency Brillouin zone, resulting in the extremely narrow band [28]. Note that there are also other narrow bands located at both sides of this extremely narrow one with larger band widths. We clarify that the superluminal group velocity does not violate Einstein's causality, the information velocity is never faster than light (see Appendix A in the End Matter).

We then explore the modes of the moiré PTC with momentum k residing away from the narrow band (gray triangle), close to the narrow band (red triangle) and on the narrow band (green triangle) labeled in Fig. 2(a), where intensity distributions of the electric displacement field $|D|^2$ with the temporal boundary condition $D(t+T) = D(t)e^{i\Omega T}$ are plotted in Fig. 2(b) for one temporal period T. For the mode located away from the narrow band, the distribution of $|D|^2$ is almost evenly distributed over the entire modulation period T. In comparison, the mode located close to the narrow band supports the field distribution tending to localize at $t = 0, T$. The temporal localization behavior becomes stronger for the mode located in the narrow band, exhibiting a periodically self-reconstructing pulse in time [see the bottom panel of Fig. 2(b)], which is a unique feature of the narrow band in a moiré PTC. We further study the modes in the vicinity of the narrow band, which is enlarged and plotted in Fig. 2(c). Three modes are considered, where one is on the narrow band (gray circle) and the other two are located at the momentum band gap (red and green circles). The corresponding $|D|^2$ are displayed in Fig. 2(d), which all exhibit the temporal localization behavior. More interestingly, as the two modes in the momentum band gap hold the positive (negative) imaginary eigenvalue, the field experiences the exponential growing (decaying) feature during the evolution, which will be shown in more detail in Fig. 4. Note that for the band gap modes with k approaching the middle of the momentum band gap, the temporal localization feature is gradually overshadowed by the growth behavior of the momentum gap [28].

The modulation parameters in time-varying $n(t)$ of moiré PTCs can be tuned to influence the narrowness of the band and the temporal localized modes. We first fix $N_1 = 15$, $N_2 = 16$, $n_{\min} = 1$ and vary the modulation strength Δn and plot the band structure as well as intensity distributions of $|D|^2$ in Figs. 3(a1) and 3(a2). Compared with the band structure with $\Delta n = 1$ in Fig. 2(a), one sees

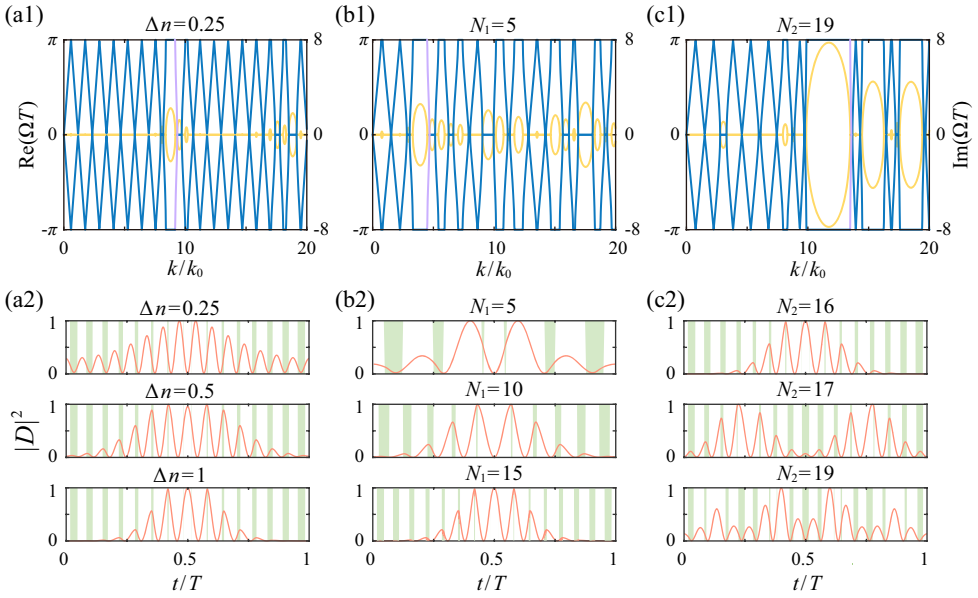

FIG. 3. Band structure of the moiré PTC with (a1) $N_1/N_2 = 15/16$ and $\Delta n = 0.25$; (b1) $N_1/N_2 = 5/6$, $\Delta n = 1$; (c1) $N_1/N_2 = 15/19$, $\Delta n = 1$. Intensity distributions of the electric displacement field $|D|^2$ for the modes at the narrow bands (violet lines) with (a2) $N_1/N_2 = 15/16$ and various Δn; (b2) $N_2 = N_1 + 1$, $\Delta n = 1$, and various N_1; (c2) $N_1 = 15$, $\Delta n = 1$, and various N_2. The shaded backgrounds in (a2) and (c2) represent the modulation pattern $n(t)$.

the band structure with $\Delta n = 0.25$, a weaker modulation strength, in Fig. 3(a1) shows that the imaginary eigenvalue $\mathrm{Im}(\Omega)$ becomes smaller and the width of the narrow band near $k = 10k_0$ is wider, which indicates a weaker localization of the temporal localized mode. A larger modulation strength Δn induces a stronger coupling between the modulation-induced sidebands, therefore opening wider momentum band gaps [21] and hence further compresses the narrow bands, making the trend for the localization of the temporal localized modes stronger, as presented in Fig. 3(a2). The modulation pattern of the moiré PTC may also lead to significant influence. In Figs. 3(b1) and 3(b2), we fix $N_2 = N_1 + 1$ and tune the parameter N_1. As N_1 increases, which references a more complicated modulation pattern, the bandwidth of the narrow band gets smaller and the localization of the temporal localized modes becomes stronger [see Figs. 2(a), 3(b1), and 3(b2)], which indicates the trend of a narrower band resulting in the stronger localization in the time domain. This can be explained by the mismatch between T_1 and T_2. As the mismatch gets smaller (i.e., increases N_1 and fixes $N_2 = N_1 + 1$), a more severe band folding in the frequency axis and a smaller frequency Brillouin zone can be expected, which naturally leads to a narrower band. However, this trend is not always true, as we show in Figs. 3(c1) and 3(c2), where we fix $N_1 = 15$ and change N_2 (so the relation $N_2 = N_1 + 1$ is breaking here). One finds that although increasing N_2 gives a more complicated modulation pattern and a narrower band [see Fig. 3(c1) for $N_2 = 19$], the intensity distribution $|D|^2$ of the modes in Fig. 3(c2) are different from the ones we have studied in previous cases. In other words, we find that such moiré PTCs also have a magic configuration inherited from the 1D spatial moiré superlattice [27,31,32], where the width of narrow band can become extremely small (a further discussion on the influence of the details in modulation patterns is given in SM [28]). Moreover, the shape of $n_1(t)$ and $n_2(t)$ can also slightly affect the narrowness of the band and the temporal localization behavior [28].

We further explore the dynamics of the temporal localized modes found in moiré PTCs with the band structure in Fig. 4(a). In Fig. 4(b) we show numerical results of the temporal evolution within five modulation periods for three modes in the vicinity of the narrow band that we have studied previously in Fig. 2(c). One finds that the modes located at the narrow band (gray circle) and the momentum band gap (red and green circles) both show a periodically temporal localization behavior. This is particularly interesting for the modes located at the momentum band gap, which are fundamentally different from the ones in conventional binary PTCs [21,22,33,34] depending on the $\mathrm{Im}(\Omega)$ of the mode. For the modes located at the momentum band gap in a conventional binary PTC, the growing (or decaying) modes always dominated during the evolution. However, beside the globally exponential growing (or decaying) trend, in each single modulation period T, the intensity of the modes still monotonically increases until it reaches its peak and then decreases, exhibiting the clear localization feature. Moreover, we investigate a mode-locking mechanism in such a moiré PTC as a temporal analog of the one in a spatial moiré superlattice where mode locking in momentum space is exhibited [9], as illustrated in Fig. 4(c). For a

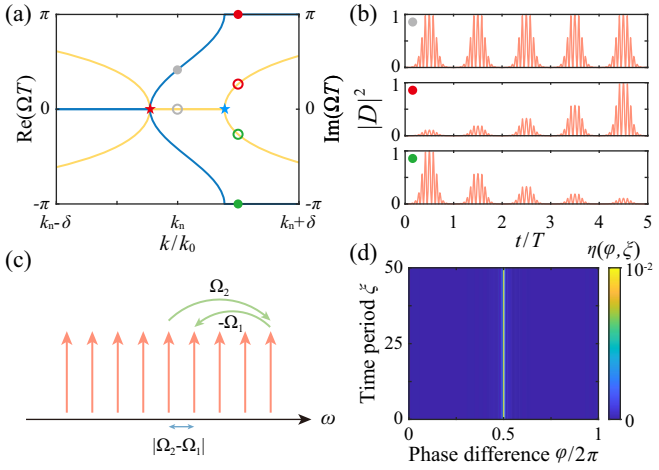

FIG. 4. Band structure of the moiré PTC with parameters same as Fig. 2(c). (b) Intensity distributions of $|D|^2$ for the modes denoted by the gray, red, and green circles in (a) within five modulation periods, respectively. The red and blue stars denote the EPs. (c) Illustration of the mode-locking mechanism. (d) Saturated distribution of $\eta(\varphi,\xi)$ versus the evolution time t with the maximum value of $\eta(\varphi,\xi)$ being 1.

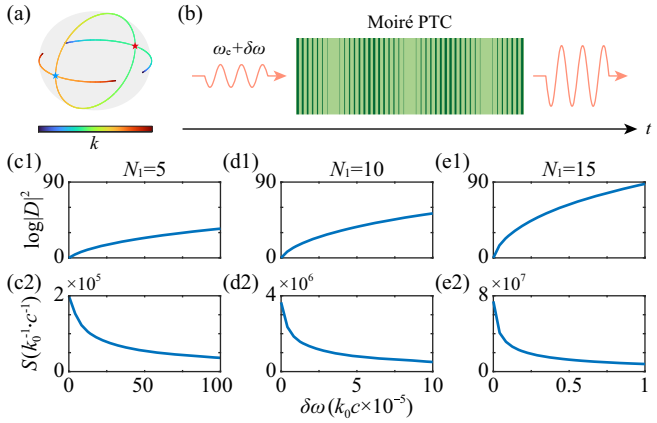

FIG. 5. (a) The eigenvectors in the Bloch sphere with k varying, where the blue and red stars denote collapsed eigenvectors corresponding to the two EPs in Fig. 4(a), respectively. (b) Illustration of probing a small frequency shift $\delta\omega$ of the input wave by a moiré PTC. (c)–(e) The output intensities of the electric displacement field $|D|^2$ and the sensitivity S versus $\delta\omega$ after the modulation of a moiré PTC, where $N_2 = N_1 + 1$ and $N_1 = 5$, 10, 15, respectively.

single-frequency modulation $n_1(t)$ with the modulation frequency Ω_1 [$n_2(t)$ with Ω_2], the Floquet modes are delocalized in the time domain, and only the Floquet modes with frequency spacing Ω_1 can be coupled. Nevertheless, once the modulation $n(t)$ is introduced, the Floquet modes with frequency spacing $|\Omega_2 - \Omega_1|$ can also be coupled with each other, which leads to the mode locking in frequency space and the pulse localization in the time domain (further illustration of the Floquet mode-locking mechanism is given in SM [28]). We further verify such a mode-locking mechanism by performing the numerical simulation within 50 modulation periods. In Fig. 4(d), we plot the saturated distribution of the density of Floquet modes $\eta(\varphi,\xi) = \lim_{\Delta\varphi\to 0}(\int_{\varphi}^{\varphi+\Delta\varphi}|A(\varphi',\xi)|d\varphi')/\Delta\varphi$. Here, $|A(\varphi',\xi)|$ represents the summation of the amplitude of the Floquet modes $|A_m|$ in the ξth modulation period, which has a phase difference $\varphi' = \mathrm{Arg}(A_m) - \mathrm{Arg}(A_{m+1})$ between adjacent frequency components. A_m is the mth frequency component, extracted from $D(t)$ in each modulation period, where we can take $t \in [(\xi-1)T, \xi T]$ and then apply a Fourier transform. One sees the distribution $\eta(\varphi,\xi)$ is invariant at each phase difference during the evolution, indicating a mode-locking signature hidden in moiré PTCs. Therefore, the proposed moiré PTCs holds the potential for developing novel thresholdless mode-locked lasers by utilizing the modes located at the momentum band gaps near the narrow band [e.g., red circle in Fig. 4(a)], which extract energy from the temporal modulation instead of a gain medium [21,22] and thus do not require external pumping [35,36]. Moreover, the extremely narrow band holds a large slope, resulting in very low density of states, which can strongly suppress the spontaneous emission rate of atoms or quantum emitters embedded in moiré PTCs [22]. The time width of the generated pulses can also be changed by varying the modulation pattern (see Appendix B).

Another interesting property of the extremely narrow band is the EPs at the band edges. As we show in Fig. 5(a), the two eigenvectors collapse at the two EPs denoted by the red and blue stars in Fig. 4(a). Owning to the Nth-root energy splitting around EPs, there has been considerable interest in the study of EP-enhanced sensing [37,38]. One typical method to further enhance the sensitivity around EPs is to construct a higher-order EP [39]. Here, we show another way to enhance the sensitivity through temporal modulation, due to the effective control of the narrowness of the band. We consider a monochromatic wave, $e^{i\omega_e t}\cos\delta\omega t$, injected in a static medium, followed by a finite modulation time of a moiré PTC. The momentum of a monochromatic wave $e^{i\omega_e t}$ is set at the exceptional point. The additional modulation $\cos\delta\omega t$ slightly shifts the momentum of the wave, and hence it falls within the momentum band gap of the moiré PTC, resulting in an amplified output wave. By measuring the amplification rate, one can detect such a small frequency shift $\delta\omega$. In Figs. 5(c1)–5(e1), we show the output intensities of the electric displacement field $|D|^2$ after the modulation of a moiré PTC with a temporal duration $30T$, where $N_2 = N_1 + 1$, and $N_1 = 5$, 10, 15, respectively. As N_1 increases, $|D|^2$ becomes larger. Moreover, the sensitivity $S = \partial(\log|D|^2)/\partial(\delta\omega)$ is increased from $\sim 10^5$ to $\sim 10^7$ when N_1 changes from 5 to 15 [see Figs. 5(c2)–5(e2)], indicating a significant enhancement of sensitivity.

In summary, we theoretically explore moiré PTCs that support extremely narrow bands and temporal localized modes. The self-reconstructing temporal localized modes

indicate the mode-locking mechanism in frequency space, which points to the potential application of mode-locked lasers with a tunable time width for the generated pulse. Compared with previous works with temporal localization behavior [21,40,41], our Letter provides a simpler strategy, and thus enables new opportunities in wave manipulations with time-varying systems. The extremely narrow band induced by dynamical modulation also opens new avenues in enhancing the sensitivity around EPs. In particular, the dynamical feature and the absence of an explicit gain medium in the proposed moiré PTC make it possible for future weakening the fundamental quantum and thermal noise compared to static EP sensors [42–44]. Recent progress in experiments shows new opportunities in realizing the proposed moiré PTCs in various platforms (see Appendix C). Our Letter provides a new direction in wave manipulations with time-varying systems, which may further extend to spatiotemporal media [45–51], leading to localized modes in both space and time domains.

Note added—Related to and independent of our work, a recent preprint [52] studying the superluminal propagation of pulses in a photonic time moiré superlattice came to our attention.

Acknowledgments—The research was supported by National Key R&D Program of China (No. 2023YFA 1407200), National Natural Science Foundation of China (12122407 and 12192252).

Data availability—The data that support the findings of this article are openly available [53].

[1] L. Du, M. R. Molas, Z. Huang, G. Zhang, F. Wang, and Z. Sun, Moiré photonics and optoelectronics, Science **379**, eadg0014 (2023).
[2] M. Oudich, X. Kong, T. Zhang, C. Qiu, and Y. Jing, Engineered moiré photonic and phononic superlattices, Nat. Mater. **23**, 1169 (2024).
[3] L. Du, Z. Huang, J. Zhang, F. Ye, Q. Dai, H. Deng, G. Zhang, and Z. Sun, Nonlinear physics of moiré superlattices, Nat. Mater. **23**, 1179 (2024).
[4] S. Sunku, G. Ni, B.-Y. Jiang, H. Yoo, A. Sternbach, A. McLeod, T. Stauber, L. Xiong, T. Taniguchi, K. Watanabe *et al.*, Photonic crystals for nano-light in moiré graphene superlattices, Science **362**, 1153 (2018).
[5] P. Wang, Y. Zheng, X. Chen, C. Huang, Y. V. Kartashov, L. Torner, V. V. Konotop, and F. Ye, Localization and delocalization of light in photonic moiré lattices, Nature (London) **577**, 42 (2020).
[6] H. Tang, F. Du, S. Carr, C. DeVault, O. Mello, and E. Mazur, Modeling the optical properties of twisted bilayer photonic crystals, Light Sci. Appl. **10**, 157 (2021).
[7] D. Yu, G. Li, L. Wang, D. Leykam, L. Yuan, and X. Chen, Moiré lattice in one-dimensional synthetic frequency dimension, Phys. Rev. Lett. **130**, 143801 (2023).
[8] C.-H. Yi, H. C. Park, and M. J. Park, Strong interlayer coupling and stable topological flat bands in twisted bilayer photonic moiré superlattices, Light Sci. Appl. **11**, 289 (2022).
[9] R.-M. Ma, H.-Y. Luan, Z.-W. Zhao, W.-Z. Mao, S.-L. Wang, Y.-H. Ouyang, and Z.-K. Shao, Twisted lattice nanocavity with theoretical quality factor exceeding 200 billion, Fund. Res. **3**, 537 (2023).
[10] X.-R. Mao, Z.-K. Shao, H.-Y. Luan, S.-L. Wang, and R.-M. Ma, Magic-angle lasers in nanostructured moiré superlattice, Nat. Nanotechnol. **16**, 1099 (2021).
[11] A. Raun, H. Tang, X. Ni, E. Mazur, and E. L. Hu, Gan magic angle laser in a merged moiré photonic crystal, ACS Photonics **10**, 3001 (2023).
[12] H.-Y. Luan, Y.-H. Ouyang, Z.-W. Zhao, W.-Z. Mao, and R.-M. Ma, Reconfigurable moiré nanolaser arrays with phase synchronization, Nature (London) **624**, 282 (2023).
[13] Q. Fu, P. Wang, C. Huang, Y. V. Kartashov, L. Torner, V. V. Konotop, and F. Ye, Optical soliton formation controlled by angle twisting in photonic moiré lattices, Nat. Photonics **14**, 663 (2020).
[14] Y. V. Kartashov, F. Ye, V. V. Konotop, and L. Torner, Multifrequency solitons in commensurate-incommensurate photonic moiré lattices, Phys. Rev. Lett. **127**, 163902 (2021).
[15] L. Huang, W. Zhang, and X. Zhang, Moiré quasibound states in the continuum, Phys. Rev. Lett. **128**, 253901 (2022).
[16] H. Qin, S. Chen, W. Zhang, H. Zhang, R. Pan, J. Li, L. Shi, J. Zi, and X. Zhang, Optical moiré bound states in the continuum, Nat. Commun. **15**, 9080 (2024).
[17] E. Lustig, O. Segal, S. Saha, C. Fruhling, V. M. Shalaev, A. Boltasseva, and M. Segev, Photonic time-crystals-fundamental concepts, Opt. Express **31**, 9165 (2023).
[18] S. Saha, O. Segal, C. Fruhling, E. Lustig, M. Segev, A. Boltasseva, and V. M. Shalaev, Photonic time crystals: a materials perspective, Opt. Express **31**, 8267 (2023).
[19] A. Boltasseva, V. Shalaev, and M. Segev, Photonic time crystals: From fundamental insights to novel applications: Opinion, Opt. Mater. Express **14**, 592 (2024).
[20] J. Reyes-Ayona and P. Halevi, Observation of genuine wave vector (k or β) gap in a dynamic transmission line and temporal photonic crystals, Appl. Phys. Lett. **107**, 074101 (2015).
[21] E. Lustig, Y. Sharabi, and M. Segev, Topological aspects of photonic time crystals, Optica **5**, 1390 (2018).
[22] M. Lyubarov, Y. Lumer, A. Dikopoltsev, E. Lustig, Y. Sharabi, and M. Segev, Amplified emission and lasing in photonic time crystals, Science **377**, 425 (2022).
[23] J. Park, H. Cho, S. Lee, K. Lee, K. Lee, H. C. Park, J.-W. Ryu, N. Park, S. Jeon, and B. Min, Revealing non-Hermitian band structure of photonic Floquet media, Sci. Adv. **8**, eabo6220 (2022).
[24] X. Wang, M. S. Mirmoosa, V. S. Asadchy, C. Rockstuhl, S. Fan, and S. A. Tretyakov, Metasurface-based realization of photonic time crystals, Sci. Adv. **9**, eadg7541 (2023).
[25] B. Lou, N. Zhao, M. Minkov, C. Guo, M. Orenstein, and S. Fan, Theory for twisted bilayer photonic crystal slabs, Phys. Rev. Lett. **126**, 136101 (2021).
[26] K. Dong, T. Zhang, J. Li, Q. Wang, F. Yang, Y. Rho, D. Wang, C. P. Grigoropoulos, J. Wu, and J. Yao, Flat bands in

magic-angle bilayer photonic crystals at small twists, Phys. Rev. Lett. **126**, 223601 (2021).
[27] D. X. Nguyen, X. Letartre, E. Drouard, P. Viktorovitch, H. C. Nguyen, and H. S. Nguyen, Magic configurations in moiré superlattice of bilayer photonic crystals: Almost-perfect flatbands and unconventional localization, Phys. Rev. Res. **4**, L032031 (2022).
[28] See Supplemental Material at http://link.aps.org/supplemental/10.1103/4lqd-z567 for the deviation of band structure, explanation of the formation of the extremely narrow band, intensity distribution of the modes at the momentum band gap, influences of the details of the modulation patterns on the band structure and influences of the shape of $n_1(t)$ and $n_2(t)$ on the band structure, and illustration of the Floquet mode-locking mechanism, which includes Ref. [29].
[29] N. C. Murphy, R. Wortis, and W. A. Atkinson, Generalized inverse participation ratio as a possible measure of localization for interacting systems, Phys. Rev. B **83**, 184206 (2011).
[30] N. Wang, Z.-Q. Zhang, and C. T. Chan, Photonic Floquet media with a complex time-periodic permittivity, Phys. Rev. B **98**, 085142 (2018).
[31] W. Wang, W. Gao, X. Chen, F. Shi, G. Li, J. Dong, Y. Xiang, and S. Zhang, Moiré fringe induced gauge field in photonics, Phys. Rev. Lett. **125**, 203901 (2020).
[32] P. Hong, L. Xu, C. Ying, and M. Rahmani, Flatband mode in photonic moiré superlattice for boosting second-harmonic generation with monolayer van der Waals crystals, Opt. Lett. **47**, 2326 (2022).
[33] S. Sadhukhan and S. Ghosh, Defect in photonic time crystals, Phys. Rev. A **108**, 023511 (2023).
[34] S. Sadhukhan and S. Ghosh, Bandgap engineering and amplification in photonic time crystals, J. Opt. **26**, 045601 (2024).
[35] K. Xu, M. Fang, J. Feng, C. Liu, K. Niu, G. Xie, and Z. Huang, Thresholdless laser based on photonic time crystals, PREPRINT (Version 1) available at Research Square (2023), 10.21203/rs.3.rs-3085133/v1.
[36] M. M. Asgari, P. Garg, X. Wang, M. S. Mirmoosa, C. Rockstuhl, and V. Asadchy, Theory and applications of photonic time crystals: A tutorial, Adv. Opt. Photonics **16**, 958 (2024).
[37] J. Wiersig, Enhancing the sensitivity of frequency and energy splitting detection by using exceptional points: Application to microcavity sensors for single-particle detection, Phys. Rev. Lett. **112**, 203901 (2014).
[38] W. Chen, Ş. Kaya Özdemir, G. Zhao, J. Wiersig, and L. Yang, Exceptional points enhance sensing in an optical microcavity, Nature (London) **548**, 192 (2017).
[39] H. Hodaei, A. U. Hassan, S. Wittek, H. Garcia-Gracia, R. El-Ganainy, D. N. Christodoulides, and M. Khajavikhan, Enhanced sensitivity at higher-order exceptional points, Nature (London) **548**, 187 (2017).
[40] Y. Pan, M.-I. Cohen, and M. Segev, Superluminal k-gap solitons in nonlinear photonic time crystals, Phys. Rev. Lett. **130**, 233801 (2023).
[41] O. Schiller, Y. Plotnik, O. Segal, M. Lyubarov, and M. Segev, Time-domain bound states in the continuum, Phys. Rev. Lett. **133**, 263802 (2024).
[42] K. Bai, J.-Z. Li, T.-R. Liu, L. Fang, D. Wan, and M. Xiao, Nonlinear exceptional points with a complete basis in dynamics, Phys. Rev. Lett. **130**, 266901 (2023).
[43] H. Loughlin and V. Sudhir, Exceptional-point sensors offer no fundamental signal-to-noise ratio enhancement, Phys. Rev. Lett. **132**, 243601 (2024).
[44] K. Bai, T.-R. Liu, L. Fang, J.-Z. Li, C. Lin, D. Wan, and M. Xiao, Observation of nonlinear exceptional points with a complete basis in dynamics, Phys. Rev. Lett. **132**, 073802 (2024).
[45] C. Caloz and Z.-L. Deck-Léger, Spacetime metamaterials—part i: General concepts, IEEE Trans. Antennas Propagat. **68**, 1569 (2019).
[46] C. Caloz and Z.-L. Deck-Leger, Spacetime metamaterials—part ii: Theory and applications, IEEE Trans. Antennas Propagat. **68**, 1583 (2019).
[47] N. Engheta, Metamaterials with high degrees of freedom: Space, time, and more, Nanophotonics **10**, 639 (2020).
[48] E. Galiffi, R. Tirole, S. Yin, H. Li, S. Vezzoli, P. A. Huidobro, M. G. Silveirinha, R. Sapienza, A. Alù, and J. B. Pendry, Photonics of time-varying media, Adv. Opt. Photonics **4**, 014002 (2022).
[49] S. Yin, E. Galiffi, and A. Alù, Floquet metamaterials, eLight **2**, 8 (2022).
[50] G. Li, D. Yu, L. Yuan, and X. Chen, Single pulse manipulations in synthetic time-frequency space, Laser Photonics Rev. **16**, 2100340 (2022).
[51] Z. Dong, X. Chen, and L. Yuan, Spatiotemporal coupled-mode equations for arbitrary pulse transformation, Phys. Rev. Res. **5**, 043150 (2023).
[52] L. Zou, H. Hu, H. Wu, Y. Long, Y. Chong, B. Zhang, and Y. Luo, Momentum flatband and superluminal propagation in a photonic time Moiré superlattice, arXiv:2411.00215.
[53] Z. Dong, Figshare (2025), 10.6084/m9.figshare.29391695.v1.
[54] L. Brillouin, *Wave Propagation and Group Velocity* (Academic Press, New York, 1960).
[55] L. J. Wang, A. Kuzmich, and A. Dogariu, Gain-assisted superluminal light propagation, Nature (London) **406**, 277 (2000).
[56] Y. Zhou, M. Z. Alam, M. Karimi, J. Upham, O. Reshef, C. Liu, A. E. Willner, and R. W. Boyd, Broadband frequency translation through time refraction in an epsilon-near-zero material, Nat. Commun. **11**, 2180 (2020).
[57] V. Pacheco-Peña, D. M. Solís, and N. Engheta, Time-varying electromagnetic media: Opinion, Opt. Mater. Express **12**, 3829 (2022).
[58] E. Lustig, O. Segal, S. Saha, E. Bordo, S. N. Chowdhury, Y. Sharabi, A. Fleischer, A. Boltasseva, O. Cohen, V. M. Shalaev *et al.*, Time-refraction optics with single cycle modulation, Nanophotonics **12**, 2221 (2023).
[59] W. Jaffray, S. Stengel, F. Biancalana, C. B. Fruhling, M. Ozlu, M. Scalora, A. Boltasseva, V. M. Shalaev, and M. Ferrera, Spatio-spectral optical fission in time-varying subwavelength layers, Nat. Photonics **19**, 558 (2025).
[60] V. Bacot, M. Labousse, A. Eddi, M. Fink, and E. Fort, Time reversal and holography with spacetime transformations, Nat. Phys. **12**, 972 (2016).
[61] B. Apffel, S. Wildeman, A. Eddi, and E. Fort, Experimental implementation of wave propagation in disordered time-varying media, Phys. Rev. Lett. **128**, 094503 (2022).

[62] E. Galiffi, G. Xu, S. Yin, H. Moussa, Y. Ra'di, and A. Alù, Broadband coherent wave control through photonic collisions at time interfaces, Nat. Phys. **19**, 1703 (2023).
[63] H. Moussa, G. Xu, S. Yin, E. Galiffi, Y. Ra'di, and A. Alù, Observation of temporal reflection and broadband frequency translation at photonic time interfaces, Nat. Phys. **19**, 863 (2023).
[64] T. R. Jones, A. V. Kildishev, M. Segev, and D. Peroulis, Time-reflection of microwaves by a fast optically-controlled time-boundary, Nat. Commun. **15**, 6786 (2024).
[65] Z. Dong, H. Li, T. Wan, Q. Liang, Z. Yang, and B. Yan, Quantum time reflection and refraction of ultracold atoms, Nat. Photonics **18**, 68 (2024).
[66] B. L. Kim, C. Chong, and C. Daraio, Temporal refraction in an acoustic phononic lattice, Phys. Rev. Lett. **133**, 077201 (2024).
[67] H. Ye, C. Qin, S. Wang, L. Zhao, W. Liu, B. Wang, S. Longhi, and P. Lu, Reconfigurable refraction manipulation at synthetic temporal interfaces with scalar and vector gauge potentials, Proc. Natl. Acad. Sci. U.S.A. **120**, e2300860120 (2023).
[68] L. Yu, H. Xue, R. Guo, E. A. Chan, Y. Y. Terh, C. Soci, B. Zhang, and Y. Chong, Dirac mass induced by optical gain and loss, Nature (London) **632**, 63 (2024).
[69] O. Y. Long, K. Wang, A. Dutt, and S. Fan, Time reflection and refraction in synthetic frequency dimension, Phys. Rev. Res. **5**, L012046 (2023).
[70] Z. Dong, X. Wu, Y. Yang, P. Yu, X. Chen, and L. Yuan, Temporal multilayer structures in discrete physical systems towards arbitrary-dimensional non-Abelian aharonov-bohm interferences, Nat. Commun. **15**, 7392 (2024).
[71] H. Yuan, W. Zhang, Z. Zhou, W. Wang, N. Pan, Y. Feng, H. Sun, and X. Zhang, Non-Hermitian topolectrical circuit sensor with high sensitivity, Adv. Sci. **10**, 2301128 (2023).
[72] C. Xiang, W. Jin, O. Terra, B. Dong, H. Wang, L. Wu, J. Guo, T. J. Morin, E. Hughes, J. Peters *et al.*, 3d integration enables ultralow-noise isolator-free lasers in silicon photonics, Nature (London) **620**, 78 (2023).
[73] T. Chen, D. Zou, Z. Zhou, R. Wang, Y. Feng, H. Sun, and X. Zhang, Ultra-sensitivity in reconstructed exceptional systems, Natl. Sci. Rev. **11**, nwae278 (2024).

End Matter

Appendix A: Superluminal group velocity and information velocity—Here, we explain the physical meaning of the superluminal group velocity and information velocity, and why the proposed moiré PTC does not violate Einstein's causality. Generally, the group velocity of a wave packet is defined by the moving speed of its center, while the information velocity is defined by the moving speed of its leading edge [54]. The group velocity may exceed the speed of light, which can be contributed from an increase in the local field by the gain [55], but the information velocity cannot. One can consider a simple scenario, where a truncated Gaussian wave packet propagates in a medium. Here, the group velocity corresponds to the motion of its peak, and the information velocity corresponds to the motion of its truncated edge. It has been shown that although the peak can move faster than light, the leading edge always moves at the speed of light. Once the peak of the wave packet approaches its edge, it slows down and travels almost exactly at the speed of light in the medium [40].

Appendix B: Tunable pulse width via dynamical modulaiton—The proposed moiré PTCs can be used to dynamically change the temporal width of the generated pulses by varying modulation pattern, which provides a reconfigurable method to generate mode-locking pulse sequence. In Fig. 6, we illustrate two ways to change the time width of the temporal localized mode in moiré PTCs. In Fig. 6(a), we set $n_{\max} = 3.19$, $n_{\min} = 1.595$, $N_1/N_2 = 10/11$ for $t \in [0, 4T]$, and $n_{\max} = 2$, $n_{\min} = 1$, $N_1/N_2 = 15/16$ for $t \in [4T, 8T]$, where the corresponding band structures $\Omega(k)$ and $\Omega'(k)$ are shown in the insets. For a second way shown in Fig. 6(b), we set the same parameters as Fig. 6(a) for $t \in [0, 1T]$ and $t \in [7T, 8T]$, while varying $n(t)$, N_1, and N_2 linearly for $t \in [1T, 7T]$. The temporal evolutions of the intensity distribution $|D|^2$ are shown in Figs. 6(a2) and 6(b2), with initial and final distributions being presented in Figs. 6(a3), 6(a4), 6(b3), and 6(b4), respectively, where the momentum of the excited modes is denoted by the red dashed line in Figs. 6(a1) and 6(b1). One can see that the final time width of the temporal localized modes in Figs. 6(a4) and 6(b4) are shortened compared with results in Figs. 6(a3) and 6(b3). Although there is a difference in the amplification ratio, one finds the manipulations of the intensity distribution $|D|^2$ under these two ways are identical by comparing the results in Figs. 6(a4) and 6(b4). Such time evolution can be understood by the state-projection physical picture. As the system holds spatial translational symmetry and breaks time-translation symmetry, where the momentum of states is conserved, the initial states on $\Omega(k)$ shall project to the final states on $\Omega'(k)$ with the same momentum k. Therefore, as long as the band structures of the last modulation period in the two ways are identical, the final intensity distribution $|D|^2$ of the modes is the same.

Appendix C: Potential experimental platforms—Because of the requirement of ultrafast temporal modulation, realizing such moiré PTCs in an optical regime is a nontrivial task [18,56–58]. Nevertheless, recent experimental progress [58,59] in transparent conducting oxides may enable new opportunities for experimental demonstrations. In addition, the proposed constructions of

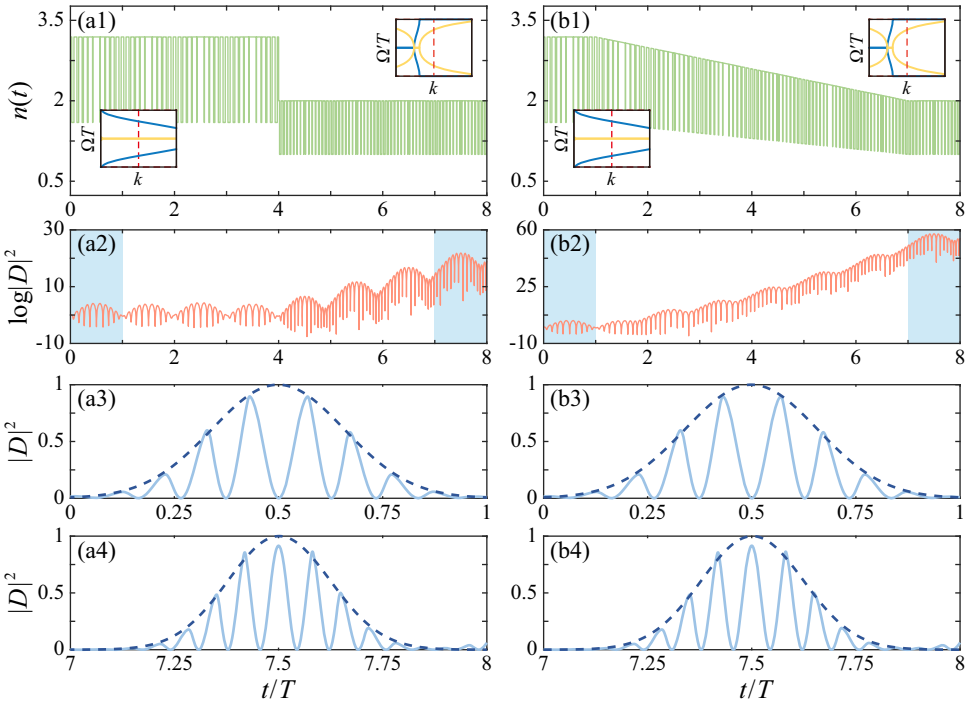

FIG. 6. (a1),(b1) Modulation pattern of the moiré PTC for $t \in [0, 8T]$. Insets show the corresponding band structures for $t \in [0, T]$ and $t \in [7T, 8T]$, respectively. (a2),(b2) Intensity distributions of $\log |D|^2$ for the modulation patterns in (a1) and (b1), respectively. Intensity distributions of $|D|^2$ for (a3),(b3) $t \in [0, T]$ and (a4),(b4) $t \in [7T, 8T]$, respectively. The dashed lines denote the envelope of $|D|^2$.

moiré PTCs are not limited in photonic systems. A proof-of-concept experiment may be feasible in different wave systems, including water waves [60,61], electric circuits and microwave systems [24,62–64], ultracold atoms [65], acoustic waves [66], time-multiplexed networks [67,68], and synthetic frequency dimensions [69,70]. For example, in the microwave system [63,64], a microwave with a carrier frequency ~1 GHz and a modulation speed ~0.1 ns are sufficient to generate the desired moiré pattern, which can be achieved by commercially available high-speed PIN photodiodes [64]. Moreover, experimental observation of the extremely narrow band may need a high resolution in the momentum axis. The inevitable dissipation and noise can broaden the extremely narrow band, which may be suppressed by applying on-chip experimental platforms [71–73].